Ring effect studies: Rayleigh scattering, including molecular parameters for rotational Raman scattering, and the Fraunhofer spectrum

Kelly V. Chance and Robert J. D. Spurr

Improved parameters for the description of Rayleigh scattering in air and for the detailed rotational Raman scattering component for scattering by O_2 and N_2 are presented for the wavelength range 200–1000 nm. These parameters enable more accurate calculations to be made of bulk molecular scattering and of the Ring effect for a variety of atmospheric radiative transfer and constituent retrieval applications. A solar reference spectrum with accurate absolute vacuum wavelength calibration, suitable for convolution with the rotational Raman spectrum for Ring effect calculations, has been produced at 0.01-nm resolution from several sources. It is convolved with the rotational Raman spectra of O_2 and N_2 to produce an atmospheric Ring effect source spectrum. © 1997 Optical Society of America

1. Introduction

The phenomenon that has come to be known as the Ring effect was first noted by Grainger and Ring[1] as a filling in (broadening and reduction of depth) of solar Fraunhofer lines when viewed from the ground in scattered sunlight. Various processes have been proposed as contributing to the effect, including scattering with fluorescence from aerosols and from the ground.[2,3] However, the predominance of molecular scattering as the major cause was established by Kattawar *et al*.,[4] who analyzed the Ring effect contributions from rotational Raman scattering and inelastic Rayleigh–Brillouin scattering. The Rayleigh–Brillouin component is not of primary importance in satellite-based UV–visible backscatter measurements for which the present study is undertaken, and it is not analyzed here. The atmospheric scattering situation is nicely defined by Young[5]: "To summarize: molecular scattering consists of Rayleigh scattering and vibrational Raman scattering. The Rayleigh scattering consists of rotational Raman lines and the central Cabannes line.   The Cabannes line is composed of the Brillouin doublet and the central Gross or Landau–Placzek line.   None of the above is completely coherent. The term 'Rayleigh line' should never be used." Note that the vibrational Raman contribution results in lines so widely separated from the frequency of the incoming light that they are not normally considered part of the Ring effect, although in recent applications the Ring effect has developed a somewhat broader definition that includes substantial interfering structure in observations, rather than the initial effect that was limited to the broadening of partially resolved lines.

Understanding the Ring effect has become more important in recent years with the increase in ultraviolet and visible spectroscopic observations of the Earth's atmosphere from the ground[6,7] and from satellites.[8–12] To retrieve abundances of trace species from such observations, it is necessary to take the Ring effect into account. Methods have been developed to do so by pragmatic means: by measuring the polarization of scattered sunlight[6] and by modeling the effect directly from molecular scattering processes.[7,10] It has been proposed to use the Ring effect with selected Fraunhofer lines (in particular, the Ca II H and K lines) to determine cloud parameters in conjunction with satellite-based observations of O_3.[11] Joiner *et al*.[10] also determined that the contribution to the Ring effect from the Rayleigh–Brillouin scattering process is negligible for most geometries used in satellite observations.

The use of visible bands of O_2, in particular the 762-nm *A* band, for determination of cloud parameters is being developed for proposed and existing satellite instruments that monitor the atmosphere with

Table 1. Relative Rayleigh and Raman Scattering Intensities[a]

V Polarization in	H Polarization in	Sum (Natural Light in)
Rayleigh–Brillouin		
$^VC_V = 180 + 4\epsilon$	$^HC_V = 3\epsilon$	$^0C_V = 180 + 7\epsilon$
$^VC_H = 3\epsilon$	$^HC_H = 3\epsilon + (180 + \epsilon)\cos^2\theta$	$^0C_H = 6\epsilon + (180 + \epsilon)\cos^2\theta$
$^VC_0 = 180 + 7\epsilon$	$^HC_0 = 6\epsilon + (180 + \epsilon)cos^2\theta$	$^0C_0 = (180 + 13\epsilon) + (180 + \epsilon)\cos^2\theta$
		$\rho_0^C = 6\epsilon/(180 + 7\epsilon)$
Raman		
$^VW_V = 12\epsilon$	$^HW_V = 9\epsilon$	$^0W_V = 21\epsilon$
$^VW_H = 9\epsilon$	$^HW_H = 9\epsilon + 3\epsilon \; \cos^2\theta$	$^0W_H = 18\epsilon + 3\epsilon \; \cos^2\theta$
$^VW_0 = 21\epsilon$	$^HW_0 = 18\epsilon + 3\epsilon \; \cos^2\theta$	$^0W_0 = 39\epsilon + 3\epsilon \; \cos^2\theta$
		$\rho_0^W = 6/7$
Sum		
$^VT_V = 180 + 16\epsilon$	$^HT_V = 12\epsilon$	$^0T_V = 180 + 28\epsilon$
$^VT_H = 12\epsilon$	$^HT_H = 12\epsilon + (180 + 4\epsilon)\cos^2\theta$	$^0T_H = 24\epsilon + (180 + 4\epsilon)\cos^2\theta$
$^VT_0 = 180 + 28\epsilon$	$^HT_0 = 24\epsilon + (180 + 4\epsilon)\cos^2\theta$	$^0T_0 = (180 + 52\epsilon) + (180 + 4\epsilon)\cos^2\theta$
		$\rho_0^T = 6\epsilon/(45 + 7\epsilon)$

[a]Mostly from Kattawar *et al.*, 1981.

emphasis on tropospheric measurements.[13] This includes the European Space Agency's global ozone monitoring experiment (GOME) and the upcoming scanning imaging absorption spectrometer for atmospheric chartography (SCIAMACHY). The Ring effect has a substantial influence on such observations; work is under way in our institution to refine and model the effects. In this case, the effect is due to inelastic scattering in molecular absorption lines themselves rather than in the solar Fraunhofer lines. Similar effects have been noted for the detailed retrieval of trace species including O_3 and NO_2.[6,7,12]

This study is part of an ongoing effort to quantify the Ring effect for atmospheric radiative transfer modeling, with application to satellite- and ground-based measurements, and to apply it to particular cases such as detailed absorption in the visible O_2 bands, the retrieval of tropospheric O_3 from UV measurements, and retrieval of trace photochemically active gases. Much of the previous modeling work[7,10,14] has relied on the development of molecular parameters for N_2 and O_2 by Penney *et al.*[15]; only one study[10] has used the updated dynamic polarizability anisotropies as developed by Bates.[16] Previous research has largely ignored the complication of the rotational Raman spectrum of O_2 caused by the electronic spin angular momentum in the $^3\Sigma_g^-$ ground state and the issue of pressure broadening of the rotational Raman lines. In this publication, we update the molecular parameters and the scattering with respect to the solar Fraunhofer spectrum using the best currently available laboratory and field data and theoretical studies of which we are aware. This provides an updated expression for Rayleigh scattering by air, expressions for the wavelength-dependent polarizability anisotropies of O_2 and N_2, accurate Placzek–Teller coefficients (the state-dependent factors in the line intensities) for O_2 rotational Raman lines (the Placzek–Teller coefficients of Penney *et al.*[15] for N_2 are correct as given), a tentative set of pressure-broadening coefficients for the O_2 and N_2 rotational Raman lines, a solar reference spectrum

for convolution with calculated Ring cross sections, and a convolved Fraunhofer-rotational Raman source spectrum for fitting of atmospheric spectra. The tables and spectra are not included here because of size limitations, but they are available from the authors.

2. Rayleigh Scattering

To examine the detailed Rayleigh and rotational Raman scattering properties, including their relative intensities and the scattering phase functions, we begin with Table I of Kattawar *et al.*,[4] which describes the relative intensities and angular behaviors for the Rayleigh–Brillouin and rotational components and their sum. They are given for various input polarizations, including unpolarized light (the predominant contribution for many atmospheric observations for which single scattering is the major contributor to the Ring effect). For unpolarized light, the depolarization ratios (defined in each case as the ratio of the horizontally polarized component to the vertically polarized component at a 90° scattering angle) can be determined directly. Table I of Kattawar *et al.*[4] is reproduced here as Table 1, with the addition of depolarization ratios for three cases: Rayleigh–Brillouin (the central Cabannes component C); rotational Raman (the wings W); and the sum of the two (T for total). The phase functions for scattering can also be derived for each case. They are (normalized over solid angle to 1)

$$\Phi_0^C = \frac{3}{160\pi}\left[\frac{(180 + 13\epsilon) + (180 + \epsilon)\cos^2\theta}{18 + \epsilon}\right],$$

$$\Phi_0^W = \frac{3}{160\pi}(13 + \cos^2\theta),$$

$$\Phi_0^T = \frac{3}{80\pi}\left[\frac{(45 + 13\epsilon) + (45 + \epsilon)\cos^2\theta}{9 + 2\epsilon}\right], \quad (1)$$

where $\epsilon = (\gamma/\bar{\alpha})^2$, γ is the anisotropy of the polarizability, and $\bar{\alpha}$ is the average polarizability. In each

case, the phase function is given in terms of the respective depolarization ratio ρ_0^X ($X = C, W, T$) by

$$\Phi_0^X = \frac{3}{8\pi}\left[\frac{(1 + \rho_0^X) + (1 - \rho_0^X)\cos^2\theta}{2 + \rho_0^X}\right]. \quad (2)$$

The Rayleigh scattering cross section at standard temperature (273.15 K) and pressure (1 atm) is given by

$$Q_R = \frac{32\pi^3(n-1)^2 F_K}{3N_0^2\lambda^4}, \quad (3)$$

where n is the index of refraction, F_K is the King correction factor,[17] N_0 is Loschmidt's number (2.686763×10^{19} cm^{-3}), and λ is the wavelength. The King correction factor is given by

$$F_K = 1 + 2\left(\frac{\gamma}{3\bar{\alpha}}\right)^2 = \frac{6 + 3\rho_0^T}{6 - 7\rho_0^T} = 1 + \frac{2\epsilon}{9}. \quad (4)$$

The average polarizability can be determined from the relation

$$|\bar{\alpha}|^2 = \frac{(n-1)^2}{4\pi^2 N_0^2}. \quad (5)$$

3. Molecular Parameters

A. Rayleigh Scattering Cross Sections

The major source of improved data for the indices of refraction of O_2, N_2, and air versus wavelength, the King correction factors, and the anisotropies of the polarizabilities is Bates.[16] He presented a comprehensive review of both measurements and theoretical calculations and derived a data set that was demonstrated to be better than 1% for all the data and parameterizations utilized in the this study.

Bates's Table 1 gives refractive indices, Rayleigh-scattering cross sections, and King correction factors versus wavelength for air from 200 to 1000 nm. We found that the following Edlén-type expression fits the index of refraction data to better than 0.1% for all values:

$$(n_{\text{air}} - 1) \times 10^4 = 0.7041 + \frac{315.90}{157.39 - \sigma^2}$$

$$+ \frac{8.4127}{50.429 - \sigma^2}, \quad (6)$$

where $\sigma(\mu m^{-1}) = 1/\lambda$ (μm). The Rayleigh cross sections are reproduced to 0.3% rms (worst case, 0.5%) over the full 0.2–1-μm range by the expression

$$Q_R \times 10^{24}(\text{cm}^2)$$

$$= \frac{3.9993 \times 10^{-4}\sigma^4}{1 - 1.069 \times 10^{-2}\sigma^2 - 6.681 \times 10^{-5}\sigma^4}. \quad (7)$$

Nicolet[18] gave an expression for fitting the data of Bates to 0.5% over the 0.2–0.55-μm range; the current expression is slightly more accurate and extends over a larger wavelength range (also see Bucholtz[19]). The

King factor and depolarization ratio for any choice of wavelength within the 0.2–1.0-μm range can be accurately determined from the previous two equations.

B. Polarizability Anisotropies

The previous expansions are for air, including standard amounts of Ar and CO_2. For rotational Raman cross sections, we limit the calculations to O_2 and N_2. Bates gave segmented representations for the indices of refraction of O_2 and N_2 versus wavelength and expansions for the respective King correction factors. Tables giving the King correction factors, values of $\sqrt{\epsilon}$, index of refraction $\bar{\alpha}$, and γ for O_2 and N_2 have been derived in this study. Values of γ_{O_2} from these data are fitted to 0.6% rms over this wavelength range (1% worst case) by

$$\gamma_{O_2} \times 10^{24} = 0.07149 + \frac{45.9364}{48.2716 - \sigma^2}. \quad (8)$$

The γ_{N_2} values are fitted to 0.02% rms (0.04% worst case) by

$$\gamma_{N_2} \times 10^{25} = -6.01466 + \frac{2385.57}{186.099 - \sigma^2}. \quad (9)$$

These equations should be considered merely as phenomenological fits over a particular wavelength range, rather than trying to attach physical importance to, for example, the negative value of the constant term in the N_2 equation. They should not be extrapolated to outside the 0.2–1.0-μm range.

C. Basic Spectroscopy

The ground state of O_2 is $^3\Sigma_g^-$; it has significant electronic structure in both its magnetic dipole rotational spectrum and its rotational Raman spectrum. Rotational Raman spectra of both O_2 and N_2 have previously been approximated by simple expansions in the lowest rotational parameters (for positions) and by using $T/c_2 B_0$ for the rotational partition functions. Precise data are now available for the term energies, allowing line positions and Boltzmann factors to be calculated accurately and rapidly. The use of term values from the current HITRAN listing[20] allows for calculations of line positions to 0.0001-cm^{-1} accuracy and for highly accurate calculation of statistical partitioning.

D. Placzek–Teller Coefficients

Cross sections for rotational Raman scattering are given by

$$Q_{N,N'}^W(\text{cm}^2) = \frac{256\pi^5}{27(\lambda')^4}\gamma^2 f_N c_{PT}(N, J, N', J'), \quad (10)$$

where f_N is the fractional population in the initial state. The quantum state-dependent factors in the cross sections $c_{PT}(N, J, N', J')$ are commonly known as Placzek–Teller coefficients from the initial derivations.[21] These factors are given for a molecule in a Σ electronic state with one electronic spin angular mo-

mentum in the Hund's case b coupling scheme (electron spin coupled to rotational angular momentum) by

$$c_{PT}(N, J, N', J') = (2N + 1)(2N' + 1)(2J' + 1)$$
$$\times \begin{pmatrix} N & L & N' \\ 0 & 0 & 0 \end{pmatrix}^2 \begin{Bmatrix} N & L & N' \\ J' & S & J \end{Bmatrix}^2,$$
(11)

where J is the total angular momentum, S is the electronic spin angular momentum (1 for O_2 and 0 for N_2), and L is the component of the 2nd rank polarizability tensor responsible for the interaction. $L = 0$ for the isotropic part of the polarizability (the Cabannes component), and $L = 2$ for the anisotropic part of the polarizability (Raman scattering). The standard definitions for 3-j and 6-j coefficients are used. Two near equivalents to this equation give the formula for line strengths. These include the initial state degeneracy.[22,23] For $S = 0$ (i.e., N_2), Eq. (11) reduces to the result of Eq. (7) in Ref. 15:

$$c_{PT}(J \rightarrow J + 2) = \frac{3(J + 1)(J + 2)}{2(2J + 1)(2J + 3)},$$

$$c_{PT}(J \rightarrow J) = \frac{J(J + 1)}{(2J - 1)(2J + 3)},$$

$$c_{PT}(J \rightarrow J - 2) = \frac{3J(J - 1)}{2(2J + 1)(2J - 1)}.$$
(12)

This derivation gives correct Placzek–Teller coefficients for N_2 but approximates those for O_2 by treating it as a pure Hund's case b molecule. At low N and J, the departures from the pure coupling case that are due to the electron spin-rotation interaction are enough to affect the spectrum significantly.[22,24] In the classic study of the O_2 ground state, Tinkham and Strandberg[25] include the correct eigenvectors of the secular determinant for levels to as high as $J = 26$ in the case b basis set (their Table V and Eq. 54). Above this level, the molecule is described by case b behavior to a high degree of accuracy. For $J = 0$ and all odd J levels, the case b description is exact. For even J levels, $J \neq 0$, the transformation from case b basis functions $\phi_{N,J}$ to eigenfunctions $\Psi_{N,J}$ is given by

$$\Psi_{J-1,J} = b_J \phi_{J-1,J} - d_J \phi_{J+1,J}$$

$$\Psi_{J+1,J} = d_J \phi_{J-1,J} + b_J \phi_{J+1,J}.$$
(13)

The b_J and d_J values from Ref. 25 are used here to calculate correct Placzek–Teller coefficients for values to as high as $J = 10$, above which the corrections become completely negligible. An almost identical result was determined by Altmann et al.,[26] who calculated eigenvectors for the secular determinant and molecular parameters given in the slightly earlier work of Mizushima and Hill.[27] The database calculated with the corrected eigenvectors is prepared with an intensity cutoff to include all rotational Raman lines with intensities at 296 K within 0.1% of the strongest line. Because of the mixing of states, this
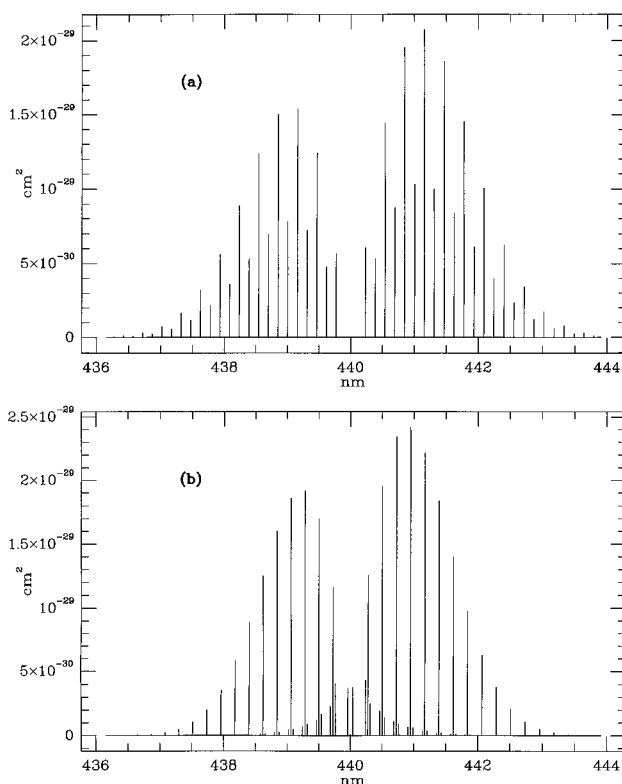

Fig. 1. Rotational Raman cross sections for (a) N_2 and (b) O_2 calculated for a temperature of 250 K and an excitation wavelength of 440 nm, appropriate to investigations of the effect of the Ring effect on retrievals of atmospheric NO_2 concentrations. The cross sections in this figure do not include the relative abundances of N_2 and O_2 in air.

now includes two $\Delta N = 4$ transitions. Figure 1 gives rotational Raman cross sections for N_2 and O_2 calculated for a temperature of 250 K and an excitation wavelength of 440 nm, appropriate to investigations of the effect of the Ring effect on retrievals of atmospheric NO_2 concentrations.

E. Pressure-Broadening Coefficients

The capital letter Γ is used here to denote the half-width at half-maximum pressure-broadening coefficient to distinguish it from the γ used for anisotropy of polarizability. The best existing measurements of pressure broadening for the rotational Raman lines are from Jammu et al.[28] who noted some evidence that the unresolved Q branches of vibrational Raman bands seem to broaden less than lines caused by ordinary dipole transitions but that the rotational Raman lines broaden comparably to dipole transitions. They present self-broadening measurements for N_2, O_2, CO_2, and CO, as well as He and Ar broadening of N_2, O_2. All the measurements were made at room temperature. Given the experimental conditions (high pressures, modest spectral resolution) and the lack of air-broadening measurements, temperature dependences, and a tabulation of the J-dependent N_2 broadening coefficients, it was decided not to use
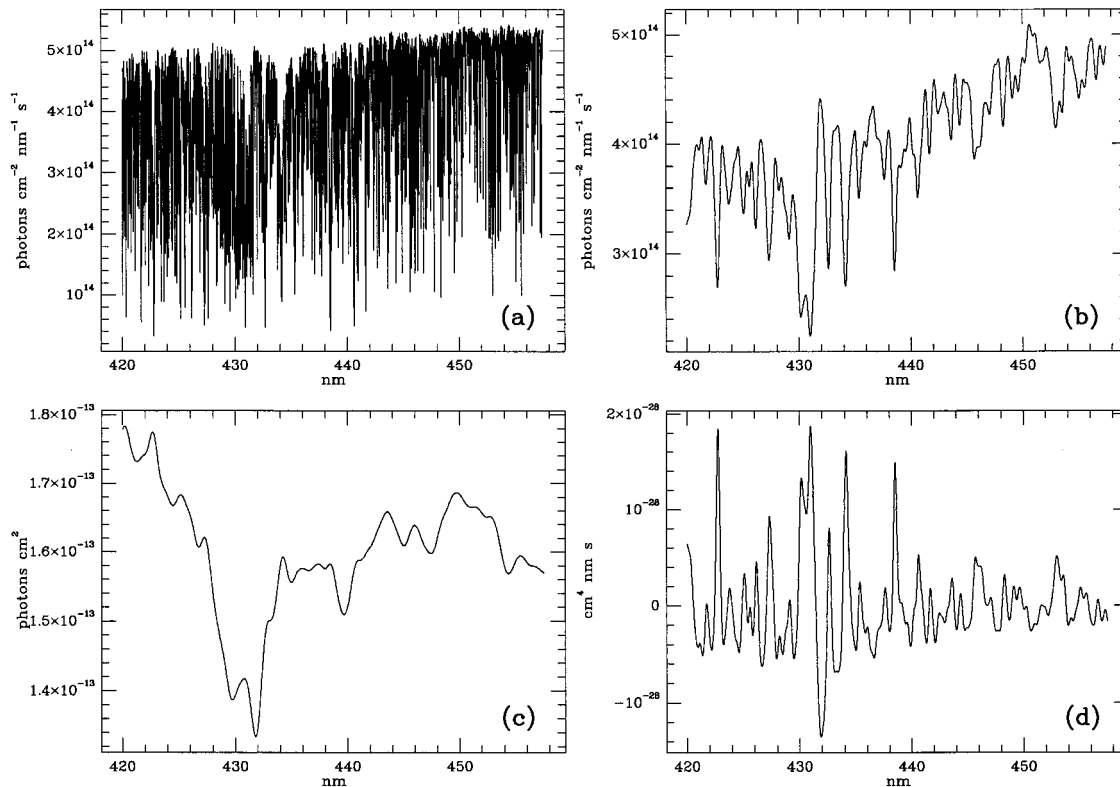
Fig. 2. (a) Sample of the Fraunhofer reference spectrum determined in this study. (b) The same Fraunhofer spectrum, convolved with a Gaussian slit function having a half-width at $1/e$ intensity of 0.212 nm, appropriate to the GOME instrument in this wavelength range. (c) The Fraunhofer spectrum of (b), convolved with the rotational Raman cross sections to create a Ring effect source spectrum. The units are those of cross section × photons, corresponding to the Ring effect scattering source per air molecule at 250 K. (d) The ratio of the Ring effect source spectrum given in (c) to the Fraunhofer spectrum of (b), with a cubic polynomial subtracted off. This spectrum closely corresponds to the Ring effect spectrum used in previous studies for atmospheric spectrum correction, as discussed in the text.

these measurements as the basis for broadening in the present data set.

For O_2, the HITRAN 92 values corresponding to rotational transitions of the same ΔN are initially adopted.[20] When multiple corresponding transitions exist, the pressure-broadening coefficients are averaged. For the two $\Delta N = 4$ transitions, the averages of the values for lines connecting the upper and lower states are taken. The resulting pressure-broadening coefficients are multiplied by 1.185, which is the average result for the ratio of measured air pressure-broadening coefficients for O_2 magnetic dipole rotational transitions to those given in HITRAN (see Ref. 29 for an explanation of this correction). For N_2, pressure-broadening values for the corresponding quadrupole lines of the vibrational fundamental are adopted. Values determined for the pressure-broadening coefficients of both O_2 and N_2 are at 296 K. The temperature dependence should be calculated using the recommended HITRAN 92 coefficient of $n = 0.5$ for N_2 lines[20] and a value of $n = 0.72$ for O_2 lines,[29] through the relation

$$\Gamma_T = \Gamma_{296}\left(\frac{296}{T}\right)^n. \tag{14}$$

4. Solar Reference and Ring Source Spectra

A solar reference spectrum for the range 230–800 nm, at 0.01 nm resolution, has been determined by combining ground-based measurements[30] and balloon measurements.[31] Both spectra were converted to vacuum wavelengths. The balloon data were recalibrated in wavelength using 20 selected atomic reference lines. The spectra were resampled at even 0.01-nm increments, employing a triangular filter of 0.01-nm half-width at half-maximum, and linearly merged over the 300–305-nm wavelength range. The result is a reference spectrum in vacuum wavelengths accurate to better than 0.001 nm above 305 nm and 0.002 nm below 300 nm. This spectrum was created specifically for GOME applications, in particular wavelength calibration studies and calculation of Ring effect contributions to GOME measurements. A sample of this Fraunhofer reference spectrum is given in Fig. 2(a); in Fig. 2(b), it has been convolved with a Gaussian slit function having a half-width at $1/e$ intensity of 0.212 nm, appropriate to the GOME instrument in this wavelength range. The solar spectrum, with GOME slit function, has been convolved with the rotational Raman cross sections described here to create a Ring effect source spectrum for fitting of GOME data. The same wavelength portion of this Ring effect source spectrum is shown in

Fig. 2(c). The units are those of cross sections times photons, corresponding to the Ring effect scattering source per air molecule at 250 K. In Fig. 2(d), the ratio of the Ring effect source spectrum to the Fraunhofer spectrum has been taken and a cubic polynomial, fitted to the region presented in the figure, has been subtracted off, for comparison with differential Ring effect spectra determined in previous studies. Atmospheric Ring spectra have been determined by several groups from polarized spectroscopic measurements of the zenith sky at high solar zenith angles. Measurements at polarizations parallel and perpendicular to the single-scattering plane are combined in similar formulations to obtain effective Ring effect cross sections.[6,7,12] For a single-scattering Rayleigh atmosphere, this procedure could yield the rotational Raman cross sections directly. In practice, because of Mie and multiple Rayleigh scattering, what is determined is the ratio of the rotational Raman spectrum to the solar Fraunhofer spectrum. This can be confirmed by comparing Fig. 2(d) with the results of the above studies. Atmospheric radiative transfer calculations of Ring spectra[7,12] also determine this quantity. It is distinct from the filling in calculated by Joiner *et al.*,[10] who include both the rotational Raman source term and the Cabannes loss term in their calculations. The use of the ratio of rotational Raman to Fraunhofer has proved useful in fitting atmospheric spectra for minor constituent abundances; it is a good approximation to the quantity needed for Ring effect correction in some fitting techniques and measurement geometries. However, its use has limitations because of the distortion of the rotational Raman spectrum and its constant ratio to the Fraunhofer spectrum. The rotational Raman spectrum and Fraunhofer spectrum determined in this study should be more generally applicable to fitting of atmospheric spectra obtained from various measurement geometries, including satellite-based measurements.

5. Conclusions

The complete Rayleigh with rotational Raman-scattering database as described in the previous sections is available from the authors. It includes N_2 and O_2 term values and statistical partitioning (tables including the quantum numbers and term energies for O_2 and N_2 up to states allowing for partitioning to better than 0.01% accuracy and Boltzmann factors with nuclear spin degeneracies g_N); tables giving the King correction factors, values of $\sqrt{\epsilon}$, where $\epsilon = (\gamma/\bar{\alpha})^2$, index of refraction $\bar{\alpha}$, and γ for O_2 and N_2; Placzek–Teller coefficients, with examples of cross sections; pressure-broadening coefficients; the solar reference spectrum derived above; and the convolved solar and rotational Raman spectrum (Ring effect source function cross section calculations). This database is a summary of the best available relevant data that were found in the literature and the calculations performed in this study. One item not included here is the additional broadening that is due to Rayleigh–Brillouin scattering.[4] For the rotational Raman lines, this will provide an extra source of broadening, although the extent of the broadening is within the uncertainties in the pressure broadening for scattering in the troposphere. The effect of Rayleigh–Brillouin scattering for the filling in of the central Cabannes line for narrow Fraunhofer lines might be significant for some satellite measurement conditions and will be a topic for future investigations.

References

1. J. F. Grainger and J. Ring, "Anomalous Fraunhofer line profiles," Nature (London) **193,** 762 (1962).
2. J. Noxon and R. Goody, "Noncoherent scattering of skylight," Izv. Acad. Sci. USSR Atmos. Oceanic Phys. **1,** 163–166 (1965).
3. D. M. Hunten, "Surface albedo and the filling-in of Fraunhofer lines in the day sky," Astrophys. J. **159,** 1107–1110 (1970).
4. G. W. Kattawar, A. T. Young, and T. J. Humphreys, "Inelastic scattering in planetary atmospheres. I. The Ring effect, without aerosols," Astrophys. J. **243,** 1049–1057 (1981).
5. A. T. Young, "Rayleigh scattering," Appl. Opt. **20,** 522–535 (1981).
6. S. Solomon, A. L. Schmeltekopf, and R. W. Sanders, "On the interpretation of zenith sky absorption measurements," J. Geophys. Res. **92,** 8311–8319 (1987).
7. D. J. Fish and R. L. Jones, "Rotational Raman scattering and the Ring effect in zenith-sky spectra," Geophys. Res. Lett. **22,** 811–814 (1995).
8. K. V. Chance, J. P. Burrows, and W. Schneider, "Retrieval and molecule sensitivity studies for the Global Ozone Monitoring Experiment and the SCanning Imaging Absorption spectroMeter for Atmospheric CHartographY," in *Remote Sensing of Atmospheric Chemistry*, J. L. McElroy and R. J. McNeal, eds., Proc. SPIE, **1491,** 151–165 (1991a).
9. J. P. Burrows, K. V. Chance, A. P. H. Goede, R. Guzzi, B. J. Kerridge, C. Muller, D. Perner, U. Platt, J.-P. Pommereau, W. Schneider, R. J. Spurr, and H. van der Woerd, *Global Ozone Monitoring Experiment Interim Science Report*, T. D. Guyenne and C. Readings, eds. Rep. ESA SP-1151, (ESA Publications Division, ESTEC, Noordwijk, The Netherlands, 1993).
10. J. Joiner, P. K. Bhartia, R. P. Cebula, E. Hilsenrath, R. D. McPeters, and H. Park, "Rotational Raman scattering (Ring effect) in satellite backscatter ultraviolet measurements," Appl. Opt. **34,** 4513–4525 (1995).
11. J. Joiner and P. K. Bhartia, "The determination of cloud pressures from rotational Raman scattering in satellite backscatter ultraviolet measurements," J. Geophys. Res. **100,** 23,019–23,026 (1995).
12. Study of the Ring Effect, Final Report, ESA Contract 10996/94/NL/CN (*ESA*, Noordwijk, The Netherlands, 1996).
13. A. Kuze and K. V. Chance, "Analysis of cloud-top height and cloud coverage from satellites using the O_2 A and B bands," J. Geophys. Res. **99,** 14,481–14,491 (1994).
14. M. Bussemer, "Der Ring-effekt: Ursachen und einfluß auf die spektroskopische messung stratosphärischer spurenstoffe," Diplomarbeit, (Universität Heidelberg, Heidelberg, Germany, 1993).

15. C. M. Penney, R. L. St. Peters, and M. Lapp, "Absolute rotational Raman cross sections for N_2, O_2, and CO_2," J. Opt. Soc. Am. **64,** 712–716 (1974).

16. D. R. Bates, "Rayleigh scattering by air," Planet. Space Sci. **32,** 785–790 (1984).

17. L. V. King, "On the complex anisotropic molecule in relation to the dispersion and scattering of light," Proc. R. Soc. London Ser. A **104,** 333–357 (1923).

18. M. Nicolet, "On the molecular scattering in the terrestrial atmosphere: an empirical formula for its calculation in the homosphere," Planet. Space Sci. **32,** 1467–1468 (1984).

19. A. Bucholtz, "Rayleigh-scattering calculations for the terrestrial atmosphere," Appl. Opt. **34,** 2765–2773 (1995).

20. L. S. Rothman, R. R. Gamache, R. H. Tipping, C. P. Rinsland, M. A. H. Smith, D. C. Benner, V. M. Devi, J.-M. Flaud, C. Camy-Peyret, A. Perrin, A. Goldman, S. T. Massie, L. R. Brown, and R. A. Toth, "The HITRAN molecular database editions of 1991 and 1992," J. Quant. Spectrosc. Radiat. Transfer **48,** 469–507 (1992).

21. G. Placzek and E. Teller, "Die rotationnstruktur der Raman-banden mehratomiger moleküle," Z. Phys. **81,** 209–258 (1933).

22. D. L. Renschler, J. L. Hunt, T. K. McCubbin, Jr., and S. R. Polo, "Triplet structure of the rotational Raman spectrum of oxygen," J. Mol. Spectrosc. **31,** 173–176 (1969).

23. M. Loëte and H. Berger, "High resolution Raman spectroscopy of the fundamental vibrational band of $^{16}O_2$," J. Mol. Spectrosc. **68,** 317–325 (1977).

24. N. H. Rich and D. W. Lepard, "Spin structure in the Raman spectrum of oxygen," J. Mol. Spectrosc. **38,** 549–551 (1971).

25. M. Tinkham and M. W. P. Strandberg, "Theory of the fine structure of the molecular oxygen ground state," Phys. Rev. **97,** 937–951 (1955).

26. K. Altmann, G. Strey, J. G. Hochenbleicher, and J. Brandmüller, "Simulation des intensitätsverlaufs im Raman-spektrum von sauerstoff unter berücksichtigung der spinaufspaltung," Z. Naturforsch. Teil A **27,** 56–64 (1972).

27. M. Mizushima and R. M. Hill, "Microwave spectrum of O_2," Phys. Rev. **93,** 745–748 (1954).

28. K. S. Jammu, G. E. St. John, and H. L. Welsh, "Pressure broadening of the rotational Raman lines of some simple gases," Can. J. Phys. **44,** 797–815 (1966).

29. K. V. Chance, W. A. Traub, K. W. Jucks, and D. G. Johnson, "On the use of O_2 spin-rotation lines for elevation angle calibration of atmospheric thermal emission spectra," Int. J. Infrared Millimeter Waves **12,** 581–588 (1991b).

30. R. L. Kurucz, I. Furenlid, J. Brault, and L. Testerman, *Solar Flux Atlas from 296 to 1300 nm* (National Solar Observatory, Sunspot, New Mexico, 1984) 240 pp.

31. L. A. Hall and G. P. Anderson, "High-resolution solar spectrum between 200 and 3100 Å," J. Geophys. Res. **96,** 12,927–12,931 (1991).